

Facing the problems on the determination of stellar temperatures and gravities: Galactic globular clusters [★]

A. Mucciarelli^{1,2} and P. Bonifacio³

¹ Dipartimento di Fisica e Astronomia, Università degli Studi di Bologna, Via Gobetti 93/2, I-40129 Bologna, Italy;

² INAF - Osservatorio di Astrofisica e Scienza dello Spazio di Bologna, Via Gobetti 93/3, I-40129 Bologna, Italy;

³ GEPI, Observatoire de Paris, Université PSL, CNRS, 5, Place Jules Janssen 92195 Meudon

March 18, 2020

ABSTRACT

We analysed red giant branch stars in 16 Galactic globular clusters, computing their atmospheric parameters both from the photometry and from excitation and ionisation balances. The spectroscopic parameters are lower than the photometric ones and this discrepancy increases decreasing the metallicity, reaching, at $[\text{Fe}/\text{H}] \sim -2.5$ dex, differences of ~ 350 K in effective temperature and ~ 1 dex in surface gravity. We demonstrate that the spectroscopic parameters are inconsistent with the position of the stars in the colour-magnitude diagram, providing too low temperatures and gravities, and predicting that the stars are up to about 2.5 magnitudes brighter than the observed magnitudes.

The parameter discrepancy is likely due to the inadequacies of the adopted physics, in particular the assumption of 1-dimensional geometry can be the origin of the observed slope between iron abundances and excitation potential that leads to low temperatures. However, the current modelling of 3D/NLTE radiative transfer for giant stars seems to be not able to totally erase this slope.

We conclude that the spectroscopic parameters are wrong for metallicity lower than -1.5 dex and for these red giant stars photometric temperatures and gravities should be adopted. We provide a simple relation to correct the spectroscopic temperatures in order to put them onto a photometric scale.

Key words. globular clusters: general — stars: abundances — stars: atmospheres — techniques: spectroscopic

1. Introduction

The determination of the atmospheric parameters (namely the effective temperature, T_{eff} , the surface gravity, $\log g$, the microturbulent velocity, v_t) is one of the most thorny aspect in the analysis of the chemical composition of FGK spectral type stars. In particular, T_{eff} covers a key role because it affects any (atomic or molecular) transition, regardless of its ionisation stage, excitation potential, strength (at variance with $\log g$ that affects mainly ionised lines and only marginally neutral ones, and v_t that affects mainly saturated lines).

T_{eff} can be directly measured if the bolometric flux and the angular diameter of the stars are known. However, due to the sub milli-arcsecond angular size of stars, measures of angular diameters are restricted to a few tens of stars (see e.g. Kervella et al. 2004; Kervella, & Fouqué 2008; Baines et al. 2008; Boyajian et al. 2008; Kervella et al. 2017). Other, indirect methods to infer T_{eff} have been developed, all of them undermined by different levels of dependence by model atmospheres (i.e. the InfraRed Flux Method, the use of Balmer line wings, the line-depth ratio).

For FGK stars T_{eff} can be derived from the photometry or directly from the spectrum. Photometric T_{eff} require dereddened broad-band colours and the adoption of suitable colour- T_{eff} transformations (see e.g. Alonso, Arribas & Martínez-Roger 1999; Ramírez & Meléndez

2005; González Hernández & Bonifacio 2009; Casagrande et al. 2010), based on the InfraRed Flux Method (hereafter IRFM, Blackwell & Shallis 1977; Blackwell et al. 1979, 1980). This widely used approach needs of accurate/precise photometry (calibrated onto same photometric system where the adopted colour- T_{eff} transformation is defined) and the knowledge of the colour excess, $E(B-V)$, as well as information about stellar metallicity, because the colour- T_{eff} relations have a mild dependence with $[\text{Fe}/\text{H}]$.

One of the most popular spectroscopic methods to infer T_{eff} in FGK stars is the so-called *excitation equilibrium*, requiring no trend between the iron abundance $A(\text{Fe})^1$ and the excitation potential χ . Two major problems can affect T_{eff} determined with this approach:

(i) low- χ lines are sensitive to T_{eff} but also to additional effects not easy to take into account, like non local thermodynamical equilibrium (NLTE) and geometry/granulation effects (see e.g. Bergemann et al. 2012; Amarsi et al. 2016);

(ii) the use of spectra with a small spectral coverage, hence with a low number of Fe I lines, makes uncertain the determination of the slope between $A(\text{Fe})$ and χ (hereafter σ_χ), decreasing significantly the accuracy and precision in the determination of T_{eff} . Additionally, the low- χ lines are on average the strongest ones (see for instance Fig. 1 in Mucciarelli et al. 2013a) leading to a degeneracy between spectroscopic T_{eff} and v_t , (the latter can be derived only spectroscopically by removing any trend between $A(\text{Fe})$ and the line strength).

[★] Based on observations collected at the ESO-VLT under the programs 065.L-0507, 072.D-0507, 073.D-0211, 078.B-0238, 081.B-0900, 083.D-0208, 085.D-0375, 089.D-0094, 093.D-0583, 095.D-0290, 188.D-3002.

¹ $A(\text{Fe}) = \log \frac{N_{\text{Fe}}}{N_{\text{H}}} + 12$

Differences between the two approaches have been already highlighted in literature, especially in the metal-poor regime where the spectroscopic T_{eff} turns out to be often lower than the photometric ones by some hundreds of K (see e.g. Johnson 2002; Cayrel et al. 2004; Cohen et al. 2008; Frebel et al. 2013; Yong et al. 2013). Such differences can lead to lower absolute abundances (by ~ 0.2 - 0.3 dex), can falsify the abundance ratios and introduce systematics that erase the precision due to the spectral quality.

In this work we analyse a representative sample of red giant branch (RGB) stars in 16 Galactic globular clusters (GCs) with the aim to compare parameters derived from the spectroscopic and photometric approaches described above and highlight possible bias in the two methods. GCs are powerful tools to perform this kind of comparison, because colour excess (fundamental to derive photometric T_{eff}), distance and stellar mass (necessary to calculate $\log g$) can be easily obtained from the isochrone-fitting of the main sequence turnoff point observed in their colour-magnitude diagram (CMD). Also, because a GC can be efficiently described as a single-age, single-metallicity population, its RGB stars follow a well-defined T_{eff} - $\log g$ relation, described by the theoretical isochrone with the corresponding cluster age and metallicity, thus providing a solid, physical reference to evaluate the reliability of the adopted parameters.

2. The spectroscopic dataset

We selected 16 Galactic GCs with the following criteria:

- (i) clusters covering the entire metallicity range of the Galactic halo GC system, between $[\text{Fe}/\text{H}] \sim -2.5$ dex and ~ -0.7 dex;
- (ii) GCs with available archival spectra secured with UVES-FLAMES mounted at the Very Large Telescope of the European Southern Observatory. This spectrograph provides a high spectral resolution ($R=47,000$) and a wide spectral coverage (Red Arm 580, 4800-6800 Å), thus providing a large number of Fe I and Fe II lines, necessary to robustly derive spectroscopic atmospheric parameters. Note that a huge sample of spectra of GC stars is available with the multi-object spectrograph GIRAFFE-FLAMES@VLT but these spectra, because of the limited spectral coverage, can not be suitable to robustly derive spectroscopic parameters, in particular for the most metal-poor GCs, due to the low number of Fe I lines (especially those with low χ) and the lack of Fe II lines;
- (iii) GCs with available ground-based UBVI photometry from the database maintained by P. B. Stetson² (see Stetson et al. 2019) and calibrated in the standard Landolt (1992) photometric system. For these clusters JK_s near-infrared photometry is available from the Two Micron All Sky Survey (2MASS, Skrutskie et al. 2006);
- (iv) GCs with relatively low colour excess ($E(B-V) < 0.2$ mag) in order to minimise the effects of differential reddening that can reduce the precision in the photometric parameters.

3. Determination of the atmospheric parameters

3.1. Photometric parameters

Photometric T_{eff} have been derived through the colour- T_{eff} transformations by González Hernández & Bonifacio (2009) that provide relations for giant stars for the broad-band colours $(B - V)_0$, $(V - K_s)_0$ and $(J - K_s)_0$. These dereddened colours

² <http://www.cadc-ccda.hia-ihp.nrc-cnrc.gc.ca/en/community/STETSON/homogeneous/>

Table 1. Spectroscopic dataset of the target globular clusters (sorted in increasing metallicity), including the number of analysed stars, the colour excess, the V-band distance modulus and the corresponding ESO program.

CLUSTER	N_{stars}	$E(B-V)$ (mag)	$(m - M)_V$ (mag)	Program
NGC 7078	13	0.090	15.44	073.D-0211
NGC 4590	13	0.065	15.23	073.D-0211
NGC 7099	19	0.050	14.78	073.D-0211 085.D-0375
NGC 6397	12	0.195	12.63	073.D-0211
NGC 5694	6	0.110	18.25	089.D-0094
NGC 5824	6	0.140	17.95	095.D-0290
NGC 5634	7	0.060	17.20	093.B-0583
NGC 6809	13	0.120	14.00	073.D-0211
NGC 6093	9	0.200	15.76	083.D-0208
NGC 1904	10	0.030	15.60	072.D-0507
NGC 6752	12	0.070	13.27	073.D-0211
NGC 288	10	0.015	14.83	073.D-0211
NGC 5904	14	0.030	14.43	073.D-0211
NGC 1851	23	0.015	15.37	188.B-3002
NGC 2808	12	0.170	15.55	072.D-0507
NGC 104	10	0.045	13.44	073.D-0211

have been obtained with the BV magnitudes from Stetson et al. (2019) and the near-infrared JK_s magnitudes from the 2MASS database (Skrutskie et al. 2006), adopting the extinction coefficients by McCall (2004). Because the 2MASS magnitudes have uncertainties larger than the optical magnitudes, especially for the farther clusters, we adopted as J and K_s magnitudes those obtained by projecting the position of each individual star on the mean ridge line of the RGB in the $(K_s, J-K_s)$ CMD.

Colour excess $E(B-V)$ and V-band distance modulus $(m - M)_V$ for each cluster have been estimated through a best-fit of the $(V, V-I)$ CMD with theoretical isochrones from the DARTMOUTH Stellar Evolution Database (Dotter et al. 2008). The derived values of $E(B-V)$ and $(m - M)_V$ for each target cluster are listed in Table 1. These values have been compared with those listed by Harris (1996, 2010 edition): we found average differences between our values and those by Harris (1996, 2010 edition) of $+0.008$ mag ($\sigma = 0.02$ mag) and $+0.07$ mag ($\sigma = 0.10$ mag) for $E(B-V)$ and $(m - M)_V$, respectively. We stress that our values have been determined in an homogeneous way, while Harris (1996, 2010 edition) presents a compilation of values derived from different sources and methods.

Surface gravities have been estimated adopting the photometric T_{eff} , a stellar mass obtained from the corresponding best-fit theoretical isochrone and the bolometric corrections calculated with the relations provided by Alonso, Arribas & Martinez-Roger (1999). Microturbulent velocities have been estimated by erasing any trend between iron abundances and reduced EWs (defined as $\log \frac{EW}{\lambda}$). Only for the cluster NGC 2808, the photometric catalog has been corrected for differential reddening.

3.2. Spectroscopic parameters

In this approach, all the stellar parameters have been estimated from the spectra, requiring to fulfil three constraints (see Mucciarelli et al. 2013a, for a detailed description of the procedure adopted here):

- (i) T_{eff} are obtained from the so-called *excitation equilibrium*,

Table 2. Average iron abundances for the target clusters derived from photometric parameters (from Fe I and Fe II lines) and from spectroscopic parameters (from Fe I lines).

CLUSTER	[Fe I/H]	σ	[Fe II/H]	σ	[Fe I/H]	σ
	(PHOTOM)		(PHOTOM)		(SPEC)	
	(dex)	(dex)	(dex)	(dex)	(dex)	(dex)
NGC 7078	-2.42	0.07	-2.40	0.04	-2.71	0.09
NGC 4590	-2.28	0.05	-2.31	0.05	-2.60	0.07
NGC 7099	-2.31	0.05	-2.32	0.05	-2.61	0.07
NGC 6397	-2.01	0.03	-2.07	0.04	-2.25	0.06
NGC 5694	-1.92	0.05	-2.03	0.09	-2.11	0.08
NGC 5824	-1.92	0.05	-2.00	0.05	-2.08	0.05
NGC 5634	-1.80	0.05	-1.87	0.03	-1.96	0.04
NGC 6809	-1.73	0.03	-1.81	0.03	-1.90	0.04
NGC 6093	-1.77	0.03	-1.78	0.02	-1.80	0.04
NGC 1904	-1.52	0.03	-1.56	0.01	-1.62	0.03
NGC 6752	-1.49	0.03	-1.66	0.03	-1.62	0.03
NGC 288	-1.23	0.04	-1.39	0.06	-1.29	0.03
NGC 5904	-1.22	0.03	-1.31	0.05	-1.24	0.03
NGC 1851	-1.12	0.03	-1.16	0.04	-1.13	0.04
NGC 2808	-1.06	0.07	-1.18	0.07	-1.09	0.06
NGC 104	-0.75	0.03	-0.76	0.04	-0.76	0.03

Table 3. Average differences between spectroscopic and photometric parameters for each target cluster. For each value the corresponding dispersion of the mean is listed.

CLUSTER	ΔT_{eff}	σ	$\Delta \log g$	σ	Δv_t	σ	$\Delta[\text{Fe}/\text{H}]$	σ
	(K)	(K)	(dex)	(dex)	(km/s)	(km/s)	(dex)	(dex)
NGC 7078	-330	56	-1.01	0.20	-0.16	0.11	-0.29	0.06
NGC 4590	-365	40	-1.08	0.13	-0.29	0.08	-0.32	0.04
NGC 7099	-352	72	-1.06	0.14	-0.24	0.14	-0.30	0.07
NGC 6397	-247	42	-0.58	0.15	-0.18	0.17	-0.24	0.05
NGC 5694	-193	33	-0.42	0.16	-0.20	0.06	-0.18	0.04
NGC 5824	-153	23	-0.47	0.06	-0.15	0.10	-0.17	0.03
NGC 5634	-174	28	-0.49	0.13	-0.11	0.04	-0.16	0.03
NGC 6809	-160	26	-0.42	0.12	-0.05	0.07	-0.17	0.03
NGC 6093	-38	35	-0.12	0.10	-0.01	0.03	-0.03	0.03
NGC 1904	-111	31	-0.32	0.12	-0.05	0.07	-0.10	0.03
NGC 6752	-153	40	-0.13	0.09	-0.08	0.06	-0.13	0.04
NGC 288	-85	23	+0.02	0.10	-0.02	0.06	-0.05	0.04
NGC 5904	-19	32	+0.09	0.08	+0.02	0.07	-0.02	0.04
NGC 1851	-25	34	-0.01	0.12	-0.01	0.06	-0.01	0.02
NGC 2808	-47	40	+0.09	0.12	+0.00	0.06	-0.02	0.04
NGC 104	-57	23	+0.01	0.11	+0.03	0.05	-0.01	0.04

requiring no trend between iron abundances and χ ($\sigma_\chi \sim 0$);

(ii) $\log g$ are obtained from the so-called *ionisation equilibrium*, requiring that neutral and single ionised Fe lines provide the same average abundance, within the corresponding uncertainties ($[\text{Fe I}/\text{Fe II}] \sim 0$);

(iii) v_t are obtained with the same approach described above for the photometric parameters.

Thanks to their high spectral quality (signal-to-noise ratio > 100), the spectra analysed in this work allow to measure ~ 100 -200 Fe I lines in each star (depending on the metallicity), well distributed both in reduced EW and χ , and 10-20 Fe II lines, providing a robust statistical ground to use this approach.

4. Chemical analysis

The chemical abundances and the spectroscopic atmospheric parameters have been obtained with the package GALA

(Mucciarelli et al. 2013a) that calculates the abundances by matching observed and theoretical EWs of unblended lines.

Neutral and single ionised iron lines have been selected by comparing any observed spectrum with a synthetic spectrum calculated with the corresponding photometric parameters and assuming the cluster iron abundances listed by Harris (1996, 2010 edition) as guess values. Synthetic spectra have been calculated with the code SYNTH (Sbordone et al. 2004; Kurucz 2005), including all the atomic and molecular transitions available in the Kurucz/Castelli database³.

Plane-parallel, 1-dimensional model atmospheres have been calculated for each star with the ATLAS9 code (Kurucz 2005) adopting local thermodynamical equilibrium (LTE) for all species and without the use of the *approximate overshooting*. All the model atmospheres have been computed by interpolating at the cluster metallicity the opacity distribution functions

³ <http://wwwuser.oats.inaf.it/castelli/linelists.html>

by Castelli & Kurucz (2003), adopting for all the clusters an α -enhanced chemical mixture but for NGC 5694 for which a solar-scaled chemical mixture is adopted (Mucciarelli et al. 2013b).

Laboratory oscillator strengths for Fe I lines are from Martin et al. (1988) and Fuhr & Wiese (2006). At variance with Fe I lines, few of Fe II lines have laboratory oscillator strengths and, even if they are accurate, they are often imprecise, with large uncertainties (see e.g. the critical discussions about the gf -values of Fe II lines in Lambert et al. (1996) and Meléndez & Barbuy 2009). For single-ionised Fe lines we adopted the oscillator strengths by Meléndez & Barbuy (2009) that included theoretical gf -values, with high precision for the components of the same multiplet, calibrated on laboratory data or on the solar spectrum.

EWs have been measured using the DAOSPEC code (Stetson & Pancino 2008) managed through the wrapper 4DAO (Mucciarelli 2013).

Strong lines, located in the flat part of the curve of growth have been excluded because they are sensitive to the velocity fields and less sensitive to the abundance. The threshold in reduced EW has been chosen depending on the cluster metallicity (higher the metallicity/lower the temperature larger the reduced EW corresponding to the starting point of the flat part of the curve of growth). Additionally, weak (noisy) lines have been excluded, as well as lines with discrepant abundances with respect to the abundance distribution from the other lines.

5. Results

5.1. Spectroscopic vs. photometric parameters

Table 2 lists the average abundances for each target cluster obtained adopting photometric (from Fe I and Fe II lines) and spectroscopic parameters (from Fe I lines only). For each abundance ratio the dispersion of the mean is quoted. All the clusters, regardless of the adopted set of parameters, exhibit small dispersions of the mean, reflecting their high level of intrinsic homogeneity of the metallicity (see e.g. Carretta et al. 2009a).

Table 3 lists for each target cluster the average differences between the spectroscopic and photometric parameters with the corresponding dispersion of the mean.

Fig. 1 shows the run of the difference between spectroscopic and photometric T_{eff} and $\log g$ (upper and lower panel, respectively) as a function of $[\text{Fe}/\text{H}]$, the latter obtained with the photometric parameters. In both panels grey squares mark individual cluster stars, while large red circles are the average value for each cluster (the errorbars indicate $1-\sigma$ dispersion of ΔT_{eff} and $\Delta \log g$). In this figure we adopted the stellar parameters and metallicities derived from $(V - K_s)_0$, one of the most used T_{eff} indicators because of its wide colour baseline (as discussed in Section 5.2, the other colours provide the same behaviour shown in Fig. 1).

Fig. 2 shows the run of the difference between spectroscopic and photometric v_t and $[\text{Fe}/\text{H}]$ (upper and lower panel, respectively) as a function of $[\text{Fe}/\text{H}]$, adopting the same symbols of Fig. 1.

The differences between spectroscopic and photometric parameters exhibit a clear run with the metallicity, with spectroscopic T_{eff} , $\log g$ and v_t that decrease with respect to the photometric values moving toward lower metallicities. In particular, for GCs with $[\text{Fe}/\text{H}] > -1.3$ dex (namely NGC 288, NGC 5904, NGC 1851, NGC 2808 and NGC 104) the two sets of parameters agree very well each other, with an average offset of about -50 K for T_{eff} , $+0.04$ for $\log g$ and $+0.01$ km/s for v_t . These differences lead to negligible changes in the derived metallicities.

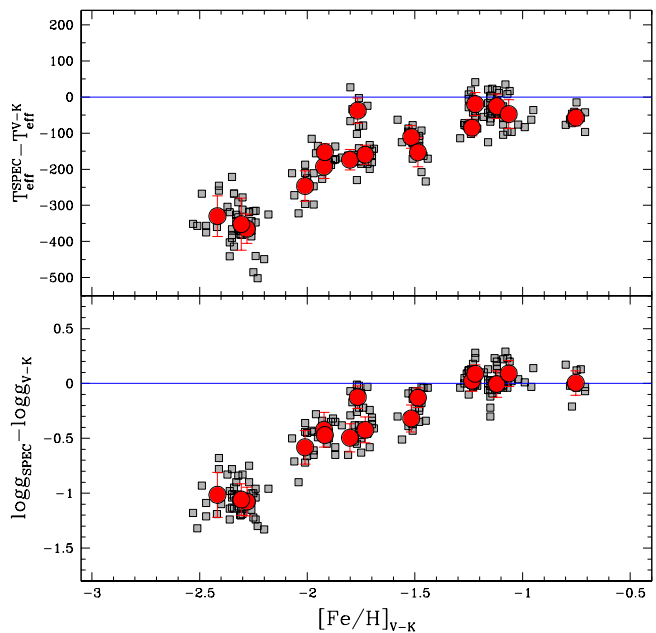


Fig. 1. Behaviour of the difference between spectroscopic and $(V - K_s)_0$ -based T_{eff} (upper panel) and $\log g$ (lower panel) as a function of the iron abundance $[\text{Fe}/\text{H}]$ derived from the photometric parameters, for individual stars (small grey squares) and average values for each cluster (red points); the errorbars indicate the $1-\sigma$ dispersion by the mean.

For the GCs with $[\text{Fe}/\text{H}]$ between -2.0 dex and -1.5 dex the spectroscopic parameters are lower than the photometric ones by ~ 100 – 200 K for T_{eff} , -0.1 – -0.5 for $\log g$ and ~ 0.0 – -0.3 dex for v_t . The $[\text{Fe}/\text{H}]$ derived from spectroscopic parameters is about 0.15 – 0.2 dex lower than those obtained with the photometric values.

Finally, for the most metal-poor clusters of the sample (namely NGC 7078, NGC 4590 and NGC 7099) the spectroscopic T_{eff} are lower by ~ 350 K, the spectroscopic $\log g$ are lower by 1 dex and v_t differ of ~ 0.3 km/s. The iron abundances derived from spectroscopic parameters are lower by ~ 0.3 dex with respect to those obtained with photometric parameters.

The lower spectroscopic T_{eff} obtained for the most metal-poor clusters arise from the significant σ_χ found when photometric T_{eff} are adopted.

As an example of the measured σ_χ , Fig. 3 shows the behaviour of Fe I abundances as a function of χ for three stars in NGC 5904, NGC 1904 and NGC 7099 when the $(V - K_s)_0$ -based T_{eff} are adopted. The values of σ_χ for the metal-rich clusters are compatible with a null slope and they become more negative decreasing the metallicity, reaching values of -0.07 – -0.10 dex/eV for the three most metal-poor target clusters.

5.2. Sanity checks

We performed some sanity checks to assess the validity of the trends discussed above.

- We repeated the analysis using photometric T_{eff} derived from the $(B - V)_0$ and $(J - K)_0$ - T_{eff} transformations provided by González Hernández & Bonifacio (2009). The average differences between spectroscopic T_{eff} and those obtained from these two additional colours are shown in

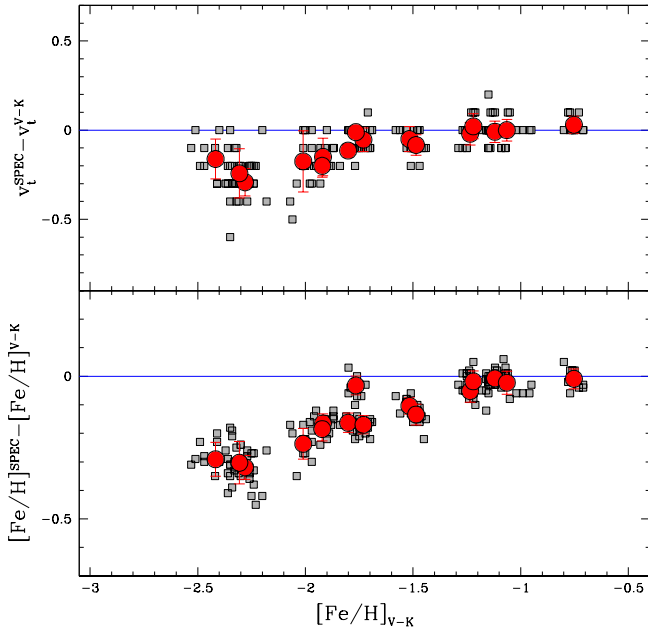


Fig. 2. Behaviour of the difference between spectroscopic and $(V - K_s)_0$ -based v_t (upper panel) and $[\text{Fe}/\text{H}]$ (lower panel) as a function of the iron abundance $[\text{Fe}/\text{H}]$ derived from the photometric parameters (same symbols of Fig. 1).

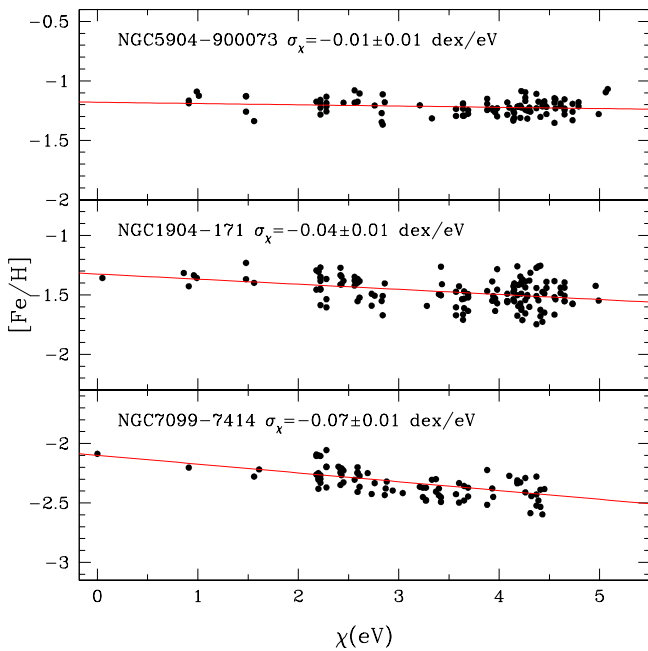


Fig. 3. Behaviour of $[\text{Fe}/\text{H}]$ as a function of χ for individual Fe I lines in three stars in NGC 5904 (upper panel), NGC 1904 (middle panel) and NGC 7099 (lower panel), adopting photometric parameters. Red lines are the linear best-fits. The slopes between $[\text{Fe}/\text{H}]$ and χ are labelled.

Fig. 4 as red circles: the behaviour with the metallicity well resembles that obtained with $(V - K_s)_0$. *The observed run of the differences of the parameters with the metallicity is independent of the adopted colours.*

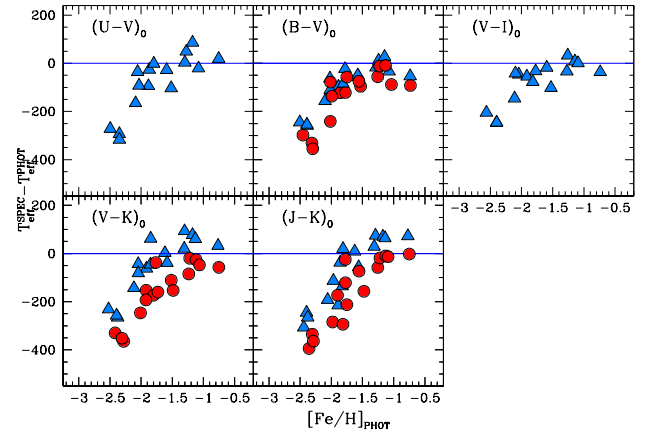


Fig. 4. As Fig. 1 adopting the relations by Alonso, Arribas & Martinez-Roger (1999, blue triangles) for the colours $(U - V)_0$, $(B - V)_0$, $(V - I)_0$, $(V - K_s)_0$ and $(J - K_s)_0$, and those by González Hernández & Bonifacio (2009, red circles) for the colours $(B - V)_0$, $(V - K_s)_0$ and $(J - K_s)_0$. Only the average values for each target cluster are shown and not the individual stars.

– We checked whether the observed trend is due to the adopted colour- T_{eff} transformations by González Hernández & Bonifacio (2009). We re-analysed the target stars using the Alonso, Arribas & Martinez-Roger (1999) relations that provide colour- T_{eff} transformations for $(U - V)_0$, $(B - V)_0$, $(V - I)_0$, $(V - K_s)_0$ and $(J - K_s)_0$. We adopted the extinction coefficients by McCall (2004), the optical UBVI magnitudes from Stetson et al. (2019) and the near-infrared JK_s magnitudes from the 2MASS survey (Skrutskie et al. 2006). The latter have been transformed into *Telescopio Carlos Sanchez* photometric system, adopted by Alonso, Arribas & Martinez-Roger (1999), using the relations by Carpenter (2001). The results are shown in Fig. 4 as blue triangles. The Alonso, Arribas & Martinez-Roger (1999) scale is cooler than that by González Hernández & Bonifacio (2009) by 47 K ($\sigma = 35$ K), 105 K ($\sigma = 11$ K) and 83 K ($\sigma = 17$ K) for $(B - V)_0$, $(V - K_s)_0$ and $(J - K_s)_0$, respectively. Despite these differences between the two scales, the same behaviour with the metallicity is found, indicating that *this run is not an artefact of the adopted T_{eff} scale.*

– The target stars have been re-analysed by excluding Fe I lines with $\chi < 2$ eV. These lines are more affected by inadequacies in the model atmospheres, in particular 3D effects (Bergemann et al. 2012; Dobrovolskas et al. 2013). A similar selection has been already adopted in other studies, even if with different thresholds (see e.g. Cayrel et al. 2004; Cohen et al. 2008; Yong et al. 2013; Ruchti et al. 2013). Spectroscopic T_{eff} derived ruling out the low-energy transitions continue to be significantly lower (by ~ 200 -300 K) than the photometric ones, for stars with $[\text{Fe I}/\text{H}] < -2.0$ dex. As clearly visible in the lower panel of Fig. 3, significant values of σ_χ (~ 0.07 -0.10 dex/eV) are found in metal-poor stars also when the low-energy Fe I lines are excluded. The inclusion of a ten of low- χ lines with higher abundances decreases v_t by ~ 0.3 km/s (because the excluded transitions are on average the strongest ones and hence the more sensitive to v_t) but has a negligible impact on the average $[\text{Fe I}/\text{H}]$, be-

cause of the large number of high-energy lines in our linelist.

- The determination of spectroscopic $\log g$ can be affected by the choice of the used gf -values of the Fe II lines, because the latter are less precise than those available for Fe I lines and laboratory values are available only for a few lines. We checked two alternative sets of Fe II gf -values, the laboratory oscillator strengths provided by Kroll & Kock (1987); Heise & Kock (1990) and Hannaford et al. (1992) and the theoretical ones by Raassen & Uylings (1998).

Gravities obtained assuming the laboratory values are compatible, within the uncertainties, with those obtained adopting the values by Meléndez & Barbuy (2009), with an average difference (laboratory - this work) of -0.03 dex ($\sigma = 0.09$ dex). On the other hand, gravities obtained with theoretical gf -values are lower than our ones, with an average difference of -0.28 dex ($\sigma = 0.13$ dex), increasing the discrepancy between the photometric and spectroscopic $\log g$. In both cases, spectroscopic T_{eff} and v_t are not affected by the choice of the gf -values of Fe II lines.

These checks demonstrate that the strong difference between spectroscopic and photometric $\log g$ shown in Fig. 1 cannot be attributed to the uncertainties in the adopted gf -values of Fe II lines.

- Finally we checked whether the adoption of a different combination of model atmospheres/spectral synthesis code can alleviate or solve the observed discrepancies. We repeated the analysis using the code TURBOSPECTRUM (Plez 2012) coupled with the MARCS model atmospheres (Gustafsson et al. 2008) but this choice does not change the observed runs.

6. Previous works

This work presents for the first time a homogeneous comparison between the two approaches used to derive stellar parameters and performed on the entire metallicity range of the Galactic GCs. The analysis of individual metal-poor clusters is not sufficient to highlight the overall behaviour that we have identified because the difference between photometric and spectroscopic parameters can be interpreted as a systematics (and not as a metallicity dependent phenomenon). However, hints of a similar behaviour have been found in some previous works analysing GCs with different metallicities.

Carretta et al. (2009b) analysed 202 giant stars in 17 GCs observed with UVES-FLAMES@VLT, adopting photometric parameters and finding that σ_χ turn out to be more negative in metal-poor stars. They provided an average slope $\sigma_\chi = -0.013$ dex/eV ($\sigma = 0.029$ dex/eV) suggesting that the photometric T_{eff} should be decreased by 45 K to obtain an average, null σ_χ . This approach interprets the average slope as the result of an offset between spectroscopic and photometric T_{eff} , while the effect becomes significant only at low metallicity. In particular, Carretta et al. (2009b) found for the GCs with $[\text{Fe}/\text{H}] < -2.0$ dex slopes of $-0.04/-0.07$ dex/eV; these values are higher than those obtained in our work with the González Hernández & Bonifacio (2009) relations but compatible with those that we found with the Alonso, Arribas & Martínez-Roger (1999) transformations (the same used by Carretta et al. 2009b).

Nidever et al. (2019) in their study on the chemical composition of Magellanic Clouds giant stars compared the iron content of 14 southern Galactic clusters observed with APOGEE-2S with the values listed by Carretta et al. (2009b). We re-

call that the analysis by Carretta et al. (2009b) is based on photometric parameters while the atmospheric parameters for the APOGEE-2S targets have been derived from the ASPCAP pipeline (García Pérez et al. 2016) by fitting the observed spectra with synthetic ones in specific spectral regions sensitive to any parameters (hence, they are spectroscopic parameters even if they have been derived with a different approach with respect to that used here). The agreement is satisfactory down to $[\text{Fe}/\text{H}] \sim -2.0$ dex, while for the most metal-poor clusters the iron abundance for the spectroscopic parameters by ASPCAP is lower by ~ 0.2 dex than the iron content derived by Carretta et al. (2009b). Because of the different wavelength range and the use of different diagnostics, the origin of this discrepancy between optical and near-infrared GC metallicities is not trivial to disentangle, in particular because no comparison about T_{eff} and $\log g$ for the stars in common is discussed. However, a more accurate comparison between the two analyses should be performed to understand whether the discrepancy highlighted by Nidever et al. (2019) for the metal-poor GCs is due to the different methods to estimate the atmospheric parameters or other effects related to the different spectral ranges. For a more detailed comparison between near-infrared spectroscopic and photometric T_{eff} we refer the reader to Mészáros et al. (2015); Jönsson et al. (2018); Masseron et al. (2019) and Mészáros et al. (2020).

Kovalev et al. (2019) analysed some open and globular clusters determining stellar parameters by comparing the observed spectra with both LTE and NLTE synthetic spectra. The differences in T_{eff} and $\log g$ between the LTE and NLTE analyses, both based on spectroscopic diagnostics and not photometric parameters, is qualitatively analogue to those obtained in this work; in particular, for clusters with $[\text{Fe}/\text{H}] < -2.0$ dex, they found that LTE spectroscopic T_{eff} and $\log g$ are lower than the NLTE ones by ~ 200 -300 K and 0.4-0.6 dex, respectively.

7. Discussion

7.1. Which parameter set should be preferred for metal-poor giant stars?

As explained in Section 1, one of the main advantages to work with GCs is that we can easily compare the atmospheric parameters (derived from photometry or spectroscopy) with the values predicted by appropriated theoretical isochrones. This provides a powerful and exemplary check to decide whether a given set of parameters is correct or not, because it should be consistent with the position of the star in the CMD.

Fig. 5 shows the position of the individual GC stars in the $T_{\text{eff}} - \log g$ diagram (red and blue circles are the photometric and spectroscopic parameters, respectively), with superimposed the corresponding best-fit theoretical DARTMOUTH isochrone. The photometric parameters well match with the those predicted by the isochrones. On the other hand, the position of the stars, when the spectroscopic parameters are adopted, shifts systematically toward lower T_{eff} and $\log g$ decreasing the cluster metallicity.

A simple argument to prefer photometric parameters is that the spectroscopic ones predict for these stars a wrong position in the $T_{\text{eff}} - \log g$ diagram. For most of the investigated GCs, the target stars are 1-3 magnitudes fainter than the RGB Tip, while the spectroscopic parameters locate them close to the Tip of the RGB.

As a simple and quantitative test, we compared the luminosities derived from the observed magnitudes with those predicted according to the spectroscopic parameters. The stellar lu-

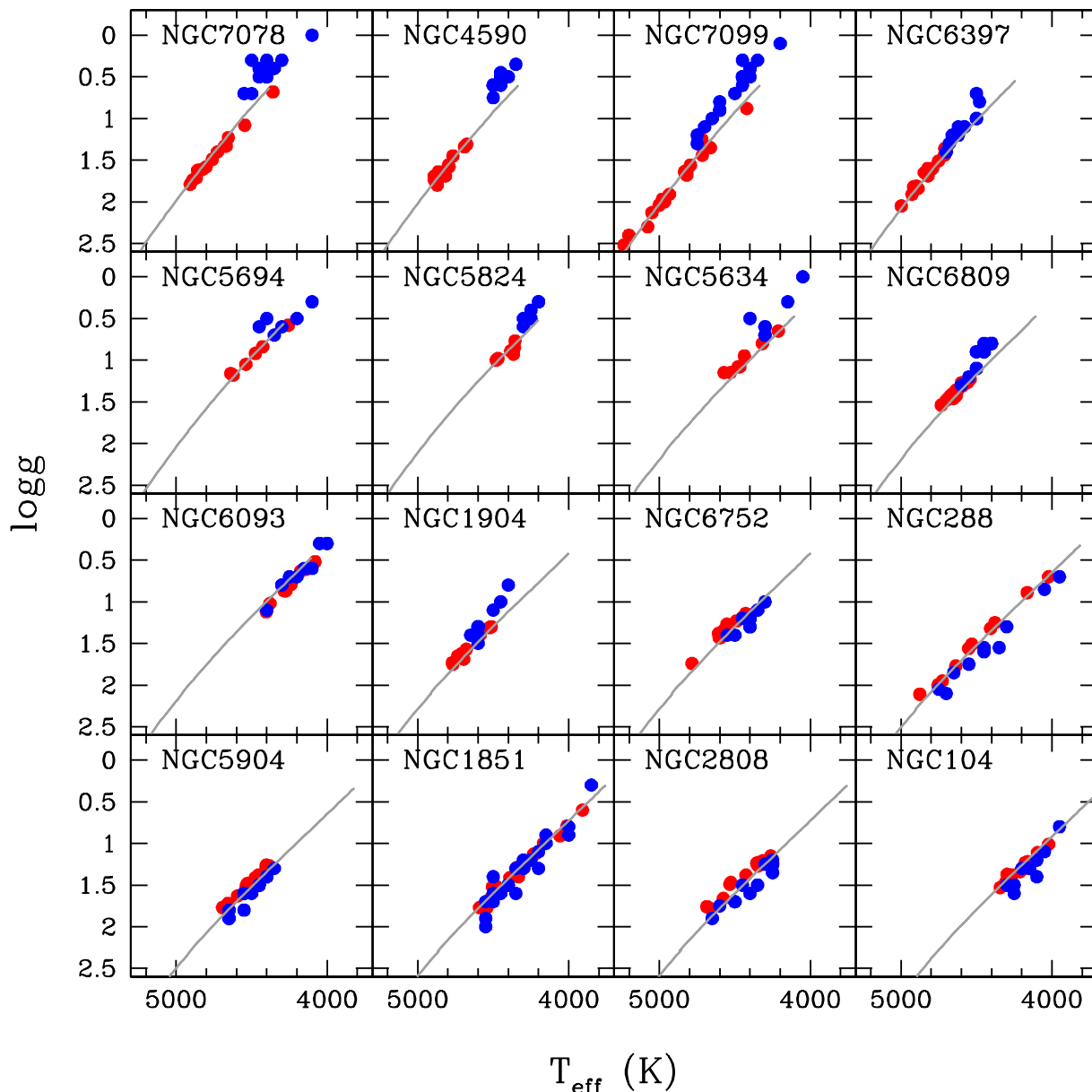


Fig. 5. Behaviour of $\log g$ as a function of T_{eff} for all the target clusters (sorted for increasing metallicity); blue points are the spectroscopic parameters and red points the photometric ones. For each cluster the corresponding best-fit DARTMOUTH theoretical isochrone is shown (grey solid line).

minosity of each target star has been calculated both from the observed V-band magnitude as described in Section 3.1, and adopting the spectroscopic T_{eff} and $\log g$. Fig. 6 shows the behaviour of the difference between the two luminosities as a function of the metallicity (the corresponding magnitude difference is also shown in the right vertical axis). Spectroscopic parameters predict luminosities higher than the observed ones and this difference increases toward lower metallicities. In terms of magnitudes, the most metal-poor GC stars should be ~ 2.5 magnitudes brighter than the observed V-band magnitudes. This demonstrates that the spectroscopic parameters for metal-poor giant stars are not consistent with the evolutionary stage of the stars as inferred from their position in the CMD. Hence, the spectroscopic parameters are not reliable locating the stars in a wrong position of the T_{eff} - $\log g$ diagram.

7.2. Technical origin of the parameter discrepancy

The discrepancy between the spectroscopic and photometric parameters is mainly driven by the discrepancy in T_{eff} that causes those also in $\log g$ and v_t (and hence in $[\text{Fe}/\text{H}]$). Fig. 7 explains how a spurious, non-null σ_χ value leads to a wrong result also in terms of $\log g$ and metallicity, locating the stars in a wrong position of the T_{eff} - $\log g$ diagram.

We consider the star NGC 4590-3584 that has photometric parameters $T_{\text{eff}} = 4831$ K and $\log g = 1.65$ (marked as a red large circle in the T_{eff} - $\log g$ diagram in the main panel of Fig. 7). The photometric T_{eff} does not satisfy the excitation equilibrium, providing a slope $\sigma_\chi = -0.09 \pm 0.01$ dex/eV, while abundances from neutral and single ionised lines are compatible each other ($[\text{Fe I}/\text{Fe II}] = 0.0$ dex).

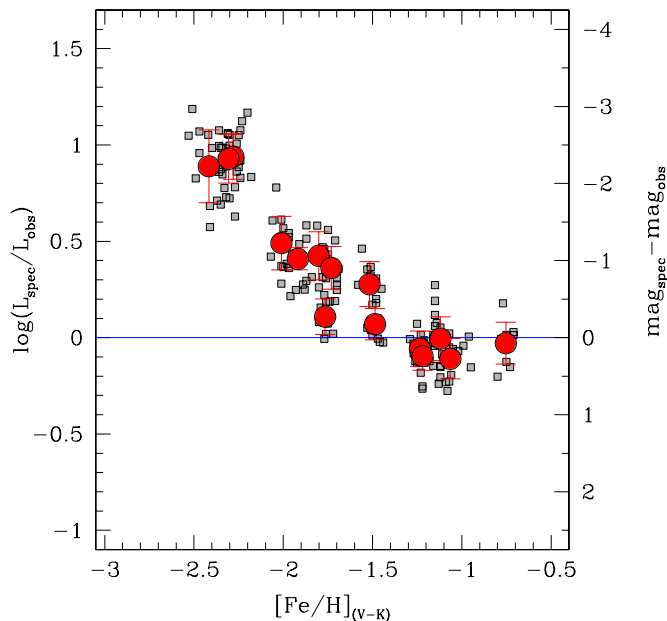


Fig. 6. Behaviour of the ratio between the luminosities derived from spectroscopic and photometric parameters as a function of $[\text{Fe}/\text{H}]$ (the latter derived from photometric parameters). The right vertical axis shows the difference in terms of magnitudes. Same symbols of Fig. 1.

In order to null σ_χ , T_{eff} needs to be decreased by ~ 400 K (green circle in the main panel). However, a change of T_{eff} impacts on both Fe I and Fe II lines but in opposite directions. In particular a decrease by 100 K decreases the abundance from Fe I lines but increases that by Fe II lines, leading to a decrease of $[\text{Fe I}/\text{Fe II}]$ by about 0.18 dex and therefore to a decrease of $\log g$ by about 0.3 dex. In the case of the star shown in Fig. 7, a decrease of ~ 400 K leads to $[\text{Fe I}/\text{Fe II}] = -0.59$ dex and we need to decrease $\log g$ by 1.2 dex in order to fulfil the ionisation equilibrium (blue circle in the main panel).

We note that the star NGC4590-3584 lies ~ 1.8 magnitudes fainter than the RGB Tip but it should be located close to the RGB Tip according to its spectroscopic parameters. This confirms that the spectroscopic parameters of this star are wrong even if they fulfil both ionisation and excitation balance.

7.3. Physical origin of the parameter discrepancy

After demonstrating that the spectroscopic parameters are not reliable for metal-poor giant stars, we should understand the physical origin of this discrepancy. The fact that the differences between the two sets of parameters increase at lower metallicities suggests that these effects are due to inadequacies of the standard model atmospheres/spectral synthesis codes and in particular the assumptions of 1D geometry and LTE.

We checked that NLTE effects, under the assumption of 1D geometry, are not sufficient to alleviate the parameter discrepancy. We applied to the Fe I lines of the three stars shown in Fig. 3 the NLTE corrections provided by Bergemann et al. (2012)⁴. We found that for the stars NGC5904-900073 and NGC1904-171 the slopes σ_χ do not significantly change, while for NGC7099-7414 a non-null σ_χ remains, indicating that a significant decrease of T_{eff} is requested also with 1D/NLTE abun-

dances. This finding is compatible with the analysis performed by Amarsi et al. (2016) of the metal-poor giant star HD122563 that shows a similar, negative σ_χ both in 1D/LTE and 1D/NLTE (see their Fig. 2).

On the other hand, 3D effects impact mainly on low χ lines (see e.g. Collet et al. 2007; Dobrovolskas et al. 2013; Amarsi et al. 2016). The star HD122563 discussed by Amarsi et al. (2016) has parameters and metallicities comparable with the most metal-poor stars studied here. The 3D/LTE analysis is able to invert the observed trend between Fe abundance and χ providing a positive σ_χ . However, the 3D/NLTE analysis provides again a negative slope (but less significant than that obtained in 1D/LTE case) because the NLTE effects counterbalance the 3D effects. The results provided by Amarsi et al. (2016) seem to suggest that a 3D/NLTE analysis could partially reduced the discrepancy between the spectroscopic and photometric parameters. However this approach still does not provide a flat behaviour between Fe abundance and χ , suggesting that our current modelling of 3D/NLTE effects in metal-poor giant stars is still incomplete.

Among the current shortcomings of available 3D model atmospheres we must recall a coarse treatment of opacity (with respect to what possible in 1D model atmospheres) and an incomplete treatment of scattering. Currently 3D model atmospheres either treat scattering as true absorption (e.g. all the older CO5BOLD models of the CIFIST grid Ludwig et al. 2009) or they use an approximate treatment, usually called the *Hayek approximation* (Hayek et al. 2010) that consists in treating scattering as true absorption in the optically thick layers and ignore it in the optically thin layers. The effects of the two approximations on the emergent fluxes are discussed in Bonifacio et al. (2018). However no investigation has been done of the impact of the different approximations on line formation. We stress that at present no grid of 3D model atmospheres with a full treatment of scattering as done by Hayek et al. (2010) is available. Another possible limitation of the current generation of the two most popular 3D model atmospheres grids, the CIFIST grid (Ludwig et al. 2009) and the STAGGER grid (Magic et al. 2013), both use the opacity package of the MARCS 1D models (Gustafsson et al. 2008), that has been created to compute models with effective temperatures below 8000 K. This implies that there are no opacities for temperatures in excess of 30 000 K. While such very high temperatures are not encountered in any layer of 1D models cooler than 8000 K, in 3D hydro models of cool stars one often finds temperatures that exceed this value, and the codes are obliged to take a bold extrapolation in the opacities.

Although there is a general consensus that NLTE effects are indeed important in the line formation of metal-poor stars we are also aware that it the calculations are more complex and must rely on input from atomic physics. Although we believe that the current NLTE computations for Fe are state-of-the art there is still the possibility that there are shortcomings. Among the ones we can think of is that some physical process that may contribute to populate or depopulate atomic levels has either been ignored, or included with an incorrect cross-section (e.g. charge transfer). A common uncertainty is provided by the collisions with neutral hydrogen. The very sophisticated calculation of Amarsi et al. (2016) did take advantage of quantum mechanical computations for the Fe+H collision rates and included charge transfer reactions that lead to $\text{Fe}^+ + \text{H}^-$, the collisions of hydrogen with Fe II had to be treated with the unphysical Drawin recipe (Drawin 1968, 1969), due to the non-availability of the relevant quantum-mechanical computations. Another issue of concern in doing NLTE computations (both in 1D or in 3D) is that the wavelength

⁴ <http://nlte.mpia.de/>

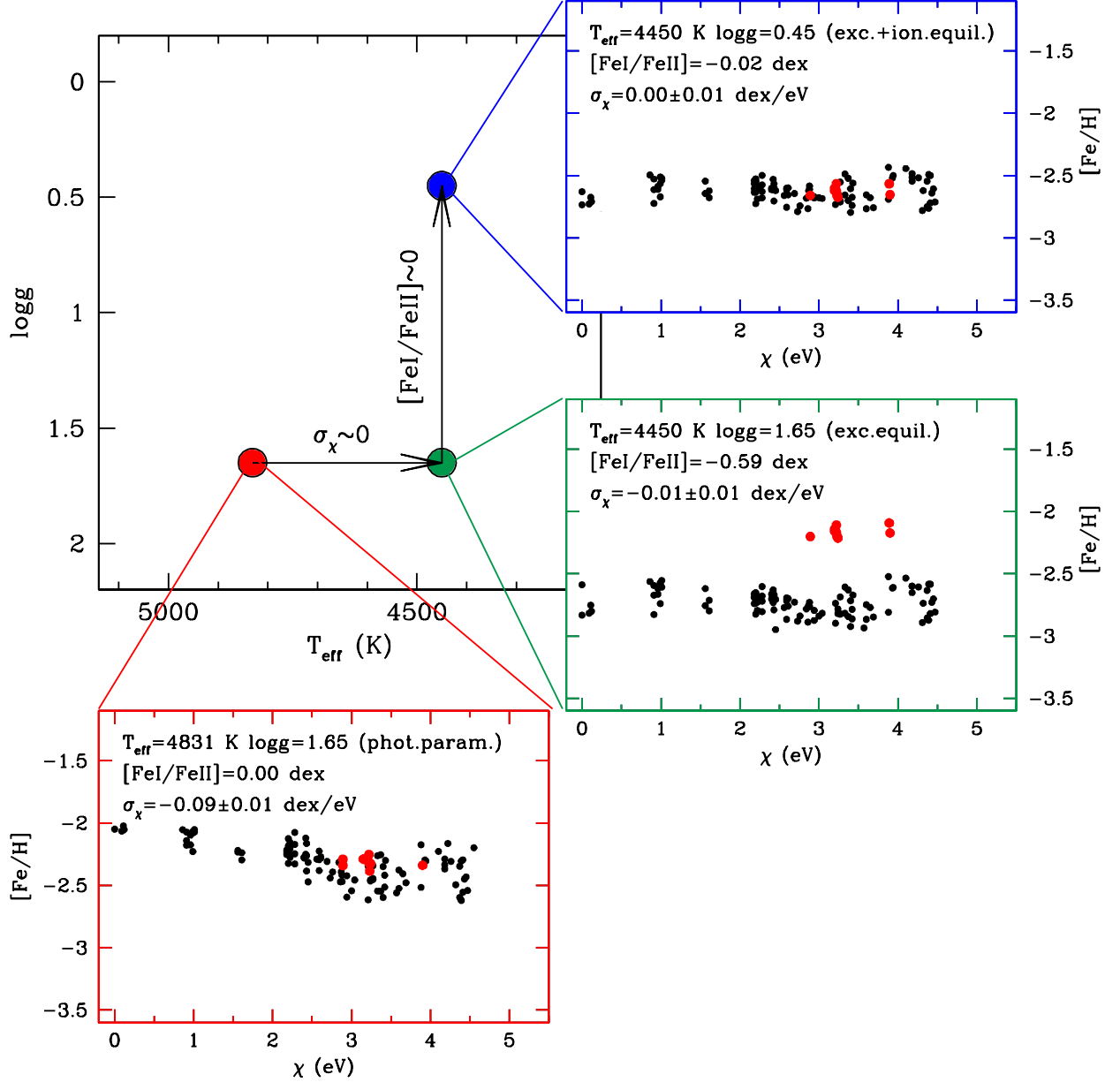


Fig. 7. Scheme of the location of the star NGC 4590-3584 in the $T_{\text{eff}}\text{-}\log g$ plane (main panel) according to different chemical analyses: the red circle indicates the photometric parameters, the green circle the position of the star when the constraint of null σ_χ is fulfilled, the blue circle the position of the star according to the spectroscopic determination of the parameters. For each of these $(T_{\text{eff}}, \log g)$ pair, the run of $[\text{Fe}/\text{H}]$ as a function of χ is shown (both neutral and single ionised lines, black and red circles respectively).

resolution must be high enough to correctly compute the wings of the strong UV lines that in many atoms effectively control the population. A computation that is too coarse may produce wrong results. Of course computations are usually checked against the Sun and Arcturus, however these checks do not guarantee that there will be any shortcoming when computing the line formation in a metal-poor giant.

A final concern is the possible effects of NLTE on the structure of a 3D model. Both CO5BOLD and STAGGER assume LTE in the model computation, NLTE is taken into account only when computing line formation, using a fixed background model. It is a reasonable assumption, but could be the cause of some shortcoming.

In our view the fact that the most advanced 3D-NLTE computations of Amarsi et al. (2016) for the metal poor giant HD 122563 are unable to remove a slope of abundance versus excitation temperature, demonstrates that even using such sophisticated computations, the excitation temperature is unreliable for a metal-poor giant.

8. A correction scheme for atmospheric parameters

As consequence of the above discussion we want to provide ready-to-use empirical recipes that will provide accurate atmospheric parameters of giant stars, that will place them in the correct place in a Hertzsprung-Russel diagram.

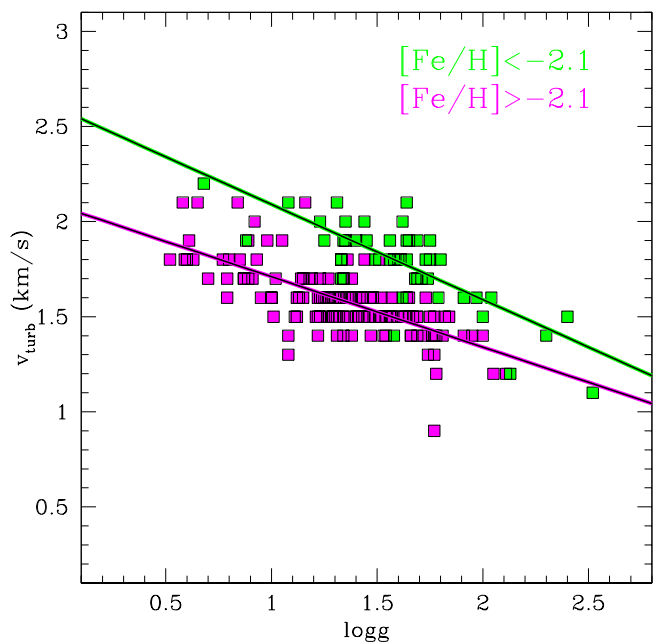


Fig. 8. Behaviour of v_t as a function of $\log g$ for the individual stars: purple and green squares are the stars in the GCs with $[\text{Fe}/\text{H}] > -2.1$ dex and $[\text{Fe}/\text{H}] < -2.1$ dex, respectively. Purple and green thick lines are the best linear fits on the two samples of stars.

8.1. RGB stars with $[\text{Fe}/\text{H}] > -1.5$ dex

For RGB stars with $[\text{Fe}/\text{H}] \gtrsim -1.5$ dex, the spectroscopic and photometric approaches are equivalent and the choice of the method is driven by the quality of the available photometry and spectra. However, the spectroscopic method should be avoided when

1. the spectral coverage does not provide a large number of Fe I lines well distributed in χ and/or line strength, introducing errors in T_{eff} and v_t ;
2. a few number of Fe II lines are available, preventing a precise determination of $\log g$.

For these stars, the lines with $\chi < 2$ eV can be used because they provide abundances coherent with those from high-energy lines, regardless of the used approach to derive T_{eff} .

Microturbulent velocities must be derived from the spectra and this parameter is heavily affected by the EW distribution of the available Fe I lines. As already done by other works (see e.g. Monaco et al. 2005; Kirby et al. 2009), we provide a linear relation between v_t and $\log g$ in order to determine this parameter also in case of spectra inadequate to this task. As visible in Fig. 8, where the run of v_t as a function of $\log g$ for all the individual stars is shown, there are two evident sequences depending on the metallicity. For the stars with $[\text{Fe}/\text{H}] > -2.1$ dex, v_t can be calculated with the following relation

$$v_{\text{turb}} = (-0.37 \pm 0.03) \cdot \log g + (2.08 \pm 0.04) \quad (\sigma = 0.13) \quad (1)$$

8.2. RGB stars with $[\text{Fe}/\text{H}] < -1.5$ dex

For RGB stars with $[\text{Fe}/\text{H}] \lesssim -1.5$ dex, the photometric approach should be always adopted, even if the available spectra allow

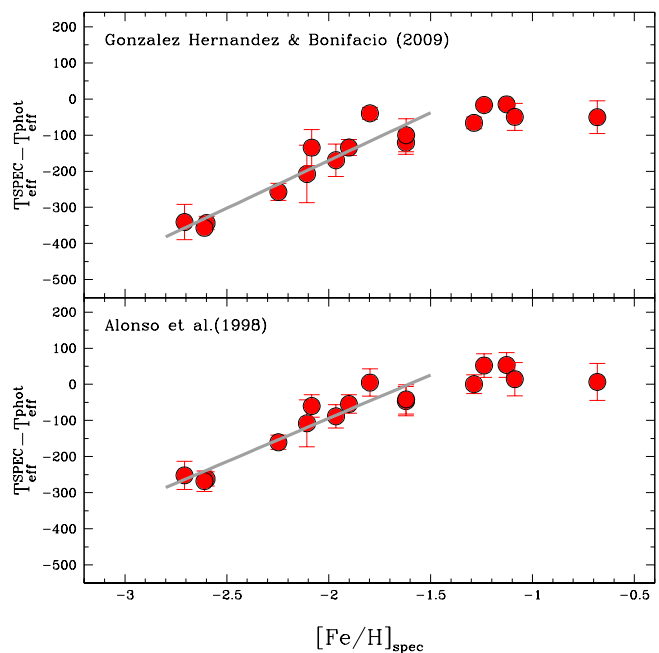


Fig. 9. Behaviour of the average difference between the spectroscopic and photometric T_{eff} obtained from individual colours for target cluster (red circles), as a function of the iron abundance derived adopting spectroscopic parameters. T_{eff} have been obtained with the relations by González Hernández & Bonifacio (2009) and Alonso, Arribas & Martínez-Roger (1999), upper and lower panel, respectively. The vertical errorbars are the dispersions of the mean of T_{eff} for each cluster. Thick grey lines are the best linear fits obtained for the clusters with $[\text{Fe}/\text{H}] < -1.5$ dex.

a precise determination of the parameters. Sometime the spectroscopic parameters can be more precise (even if less accurate) than the photometric ones because of the low quality of the available photometry, the uncertainty in the colour excess or the presence of differential reddening. For these cases, the spectroscopic parameters can be the only feasible route. In order to bypass the issues in the spectroscopic parameters discussed above, we provide a linear relation between the iron abundance obtained with the spectroscopic parameters $[\text{Fe}/\text{H}]_{\text{SPEC}}$ and the average ΔT_{eff} from the broad-band colours, both using the relations by González Hernández & Bonifacio (2009) and Alonso, Arribas & Martínez-Roger (1999), upper and lower panel in Fig. 9 respectively.

$$T_{\text{eff}}^{\text{GB09}} = T_{\text{eff}}^{\text{SPEC}} - (264 \pm 33) \cdot [\text{Fe}/\text{H}]_{\text{SPEC}} - (358 \pm 70) \quad (\sigma = 36\text{K}) \quad (2)$$

$$T_{\text{eff}}^{\text{A99}} = T_{\text{eff}}^{\text{SPEC}} - (240 \pm 28) \cdot [\text{Fe}/\text{H}]_{\text{SPEC}} - (385 \pm 60) \quad (\sigma = 31\text{K}) \quad (3)$$

Note that the relations by Alonso, Arribas & Martínez-Roger (1999) provide an excellent match with the spectroscopic T_{eff} for stars with $[\text{Fe}/\text{H}] > -1.5$ dex, while an offset of ~ 50 K remains when we use González Hernández & Bonifacio (2009). On the other hand, Alonso, Arribas & Martínez-Roger (1999) provide too low T_{eff} for the metal-poor clusters with respect to theoretical isochrones, while González Hernández & Bonifacio (2009) provide a good match with the isochrones for each metallicity.

Because these relations are defined only for RGB stars in the metallicity range $-2.5 < [\text{Fe}/\text{H}] < -1.5$ dex, we checked whether they work also at lower metallicities. We analysed 4 RGB field stars with metallicities between ~ -3.5 and ~ -2.5 dex, namely HE 0305-452, CD 38245, HD 122563 and HE 2141-3741. For these stars we retrieved archival spectra acquired with the spectrograph UVES@VLT, adopting the photometry available in the SIMBAD database (Wenger et al. 2000), colour excess from Schlafly, & Finkbeiner (2011) and parallaxes from Gaia Data Release 2 (Gaia Collaboration et al. 2016, 2018). Photometric and spectroscopic parameters and corresponding $[\text{Fe I}/\text{H}]$ are listed in Table 4. Also for these stars, significant slopes σ_χ are found when the photometric T_{eff} are adopted, leading to lower spectroscopic T_{eff} . Additionally, the spectroscopic $\log g$ are significantly lower, by about 1 dex, than the photometric ones. The precision of the Gaia parallaxes is of about 20% for HE 0305-452, CD 38245 and HE 2141-3741, and 3% for HD 122563. However, the precision of the parallax in the first three stars change the photometric gravities by about 0.2 dex and they are not able to reconcile photometric and spectroscopic $\log g$. The spectroscopic T_{eff} corrected with the relations defined from GCs well match with the photometric T_{eff} , demonstrating that these relations can be extrapolated at lower metallicities and used for very metal-poor RGB field stars (at least down to $[\text{Fe}/\text{H}] \sim -3.5$ dex), especially when no precise photometry and/or colour excess are available.

Concerning the determination of the gravities, for $[\text{Fe}/\text{H}] < -1.5$ dex, spectroscopic $\log g$ should be avoided, because the $[\text{Fe I}/\text{Fe II}]$ ratio is more sensitive to T_{eff} than to $\log g$. Hence, if the spectroscopic T_{eff} is wrong also the spectroscopic $\log g$ turns out to be wrong, due to the opposite sensitivity of Fe I and Fe II by T_{eff} (see Fig. 7). A more robust and safe approach is to use the $T_{\text{eff}}-\log g$ relation provided by a theoretical isochrone (when the age is well known as in the case of a GC) or to recalculate gravities adopting the corrected T_{eff} . In this case we give a warning, to derive $\log g$ a rough estimate of the mass of the star is needed. If we exclude the cases for which the mass is otherwise known (binary stars, stars with asteroseismic data...), the mass estimate hinges on the age estimate. If we know the star is old (say older than 10 Gyr), as in the case of GCs, we can safely assume a mass of $\sim 0.7-0.8 M_\odot$. If however the star is younger than 1 Gyr its mass can be as large as $5 M_\odot$ leading to a difference of 0.7 dex in the estimated gravity for the same effective temperature (see Lombardo et al. 2020, in preparation).

Concerning the determination of v_t , the stars down to $[\text{Fe}/\text{H}] \sim -2.1$ dex follow the same linear relation provided above, while for the stars in the three most metal-poor GCs (NGC 7078, NGC 4590 and NGC 7099, $[\text{Fe}/\text{H}] < -2.1$ dex) we provide the following relation

$$v_{\text{turb}} = (-0.50 \pm 0.06) \cdot \log g + (2.59 \pm 0.10) \quad (\sigma = 0.14) \quad (4)$$

This different behaviour for the most metal-poor stars is due to the largest T_{eff} discrepancy observed among these stars (see Fig. 1): because the low- χ lines are the strongest ones, v_t is increased to partially compensate the negative slope between abundances and χ .

Finally, we note that for these stars the lines with low-energy (< 2 eV) should be used with caution. As discussed above, the inclusion of a ten of low- χ Fe I lines does not significantly impact on the average $[\text{Fe I}/\text{H}]$ (at least for the optical spectra investigated here where the bulk of the Fe I lines includes high- χ lines). However, this cut can impact on the abundance of other species for which mainly low- χ could be available. For instance,

in the optical range covered by the UVES-FLAMES spectra discussed in this work, almost all the Ti lines have $\chi < 2$ eV and the adoption of a threshold in χ can dramatically impact on its abundance.

Finally, we recall that Ti provides a significant number of neutral and single-ionised lines, providing an additional diagnostic for the gravities. When the spectroscopic parameters are used, and $[\text{Fe I}/\text{H}]$ and $[\text{Fe II}/\text{H}]$ are consistent within the uncertainties by construction, $[\text{Ti I}/\text{H}]$ is lower by about 0.2 dex with respect to $[\text{Ti II}/\text{H}]$. This implies that the gravities should be further decreased in order to match $[\text{Ti I}/\text{H}]$ and $[\text{Ti II}/\text{H}]$, worsening the discrepancy with the photometric values. We suspect that this behaviour is due to the low χ of all the available Ti lines. The latter are extremely sensitive to the inadequacies of the model atmospheres, in particular to NLTE effects, as demonstrated by Mashonkina et al. (2016), finding that, at $[\text{M}/\text{H}] = -2.0$ dex, the NLTE corrections for the Ti I lines are larger than those for the Fe I lines.

9. Summary and conclusions

The analysis of a sample of 16 Galactic GCs observed with UVES-FLAMES@VLT using two different approaches to derive the parameters leads to the following results:

- the discrepancy between spectroscopic and photometric parameters for giant stars increases decreasing the metallicity. This behaviour is confirmed adopting different broad-band colours or colour- T_{eff} transformations. Such a difference between the two sets of parameters cannot be treated as a simple systematic;
- the spectroscopic approach based on excitation and ionisation balances provides wrong stellar parameters for metal-poor stars, in particular leading to too low T_{eff} and $\log g$, inconsistent with the values predicted by appropriate theoretical isochrones and with the observed position of the stars in the CMD;
- the discrepancy between the two approaches seems to arise from the inadequacies of the adopted physics. In particular, low-energy lines are the most prone to 3D effects (Bergemann et al. 2012; Dobrovolskas et al. 2013; Amarsi et al. 2016) and the use of 1D model atmospheres is likely responsible of the negative values of σ_χ that lead to too low T_{eff} and $\log g$. On the other hand, neither 1D/NLTE nor 3D/NLTE are sufficient to flatten the observed σ_χ and alleviate the discrepancy between the two parameter sets, at least in the computations currently available;
- we proposed simple relations to correct spectroscopic T_{eff} and put them onto "photometric" scales by Alonso, Arribas & Martínez-Roger (1999) and González Hernández & Bonifacio (2009). These relations are suitable for the RGB stars with $[\text{Fe}/\text{H}] < -1.5$ dex and they can be used to correct spectroscopic T_{eff} both in GCs and in field stars when no accurate/precise photometry are in hand;
- 1D (LTE or NLTE) chemical analyses of RGB stars with $[\text{Fe}/\text{H}] < -1.5$ dex and based on spectroscopic parameters should be considered with great caution because the parameters should be underestimated, as well as the derived $[\text{Fe}/\text{H}]$. We recommend to avoid for these stars spectroscopic T_{eff} and prefer photometric or corrected T_{eff} .

Finally, we stress that both spectroscopic and photometric T_{eff} fail to well reproduce that spectral properties of giant stars.

Table 4. Field metal-poor giant stars with the atmospheric parameters and [Fe I/H] derived adopting photometric and spectroscopic parameters.

STAR	T_{eff}	$\log g$ (A99)	[Fe I/H]	T_{eff}	$\log g$ (GHB09)	[Fe I/H]	T_{eff}	$\log g$ (SPEC)	[Fe I/H]	PROGRAM
HE0305-4520	4801	1.06	-3.05	4896	1.11	-2.96	4300	0.40	-3.50	078.B-0238
HE1116-0634	4649	1.27	-3.44	4673	1.28	-3.40	4100	0.30	-3.84	081.B-0900
HD122563	4677	1.37	-2.71	4790	1.43	-2.60	4300	0.40	-3.03	065.L-0507
HE2141-3741	5100	1.58	-3.16	5217	1.63	-3.05	4650	0.50	-3.55	078.B-0238

Spectroscopic T_{eff} provide, by construction, the same abundance from lines of different χ but clearly fail to reproduce the emerging flux of the stars. On the other hand, IRFM photometric T_{eff} well reproduce the bolometric flux but they provide systematically erroneous abundances for the low-energy lines. In 1D chemical analysis we need to decide which aspect we want to privilege, a temperature able to reproduce either the emerging stellar flux or the depth of individual metallic lines.

Our argumentation about the position of the stars in the $T_{\text{eff}} - \log g$ diagram discussed in Section 5 demonstrates that the spectroscopic T_{eff} should be rejected, while the photometric ones, despite the failure to reproduce the excitation balance, are the best choice.

However, the development of more accurate and complete 3D/NLTE tools remains the main way to obtain an exhaustive description of the stellar spectra and bypass the issues discussed in this work.

Acknowledgements. We are grateful to the anonymous referee for the useful comments and suggestions. AM is grateful to the Scientific Council of Observatoire de Paris that funded his extended visit at GEPI, where part of this work was carried out. This research has made use of the SIMBAD database, operated at CDS, Strasbourg, France and of data from the European Space Agency (ESA) mission *Gaia* (<https://www.cosmos.esa.int/gaia>), processed by the *Gaia* Data Processing and Analysis Consortium (DPAC, <https://www.cosmos.esa.int/web/gaia/dpac/consortium>). Funding for the DPAC has been provided by national institutions, in particular the institutions participating in the *Gaia* Multilateral Agreement.

References

Alonso, A., Arribas, S., & Martinez-Roger, C., 1999, *A&As*, 140, 261
 Amarsi, A. M., Lind, K., Asplund, M., et al. 2016, *MNRAS*, 463, 1518
 Baines, E. K., McAlister, H. A., ten Brummelaar, T. A., et al. 2008, *ApJ*, 682, 577
 Bergemann, M., Lind, K., Collet, R., et al. 2012, *MNRAS*, 427, 27
 Blackwell, D. E., & Shallis, M. J. 1977, *MNRAS*, 180, 177
 Blackwell, D. E., Shallis, M. J., & Selby, M. J. 1979, *MNRAS*, 188, 847
 Blackwell, D. E., Petford, A. D., & Shallis, M. J. 1980, *A&A*, 82, 249
 Bonifacio, P., Caffau, E., Ludwig, H.-G., et al. 2018, *A&A*, 611, A68
 Boyajian, T. S., McAlister, H. A., Baines, E. K., et al. 2008, *ApJ*, 683, 424
 Cayrel, R., Depagne, E., Spite, M., et al. 2004, *A&A*, 416, 1117
 Carpenter, J. M. 2001, *AJ*, 121, 2851
 Carretta, E., Bragaglia, A., Gratton, R., et al. 2009, *A&A*, 508, 695
 Carretta, E., Bragaglia, A., Gratton, R., & Lucatello, S. 2009, *A&A*, 505, 139
 Casagrande, L., Ramírez, I., Meléndez, J., Bessell, M., & Asplund, M. 2010, *A&A*, 512, A54
 Castellì, F., & Kurucz, R. L. 2003, *Modelling of Stellar Atmospheres*, 210, A20
 Cohen, J. G., Christlieb, N., McWilliam, A., et al. 2008, *ApJ*, 672, 320.
 Collet, R., Asplund, M., & Trampedach, R. 2007, *A&A*, 469, 687
 Dobrovolskas, V., Kučinskas, A., Steffen, M., et al. 2013, *A&A*, 559, A102
 Dotter, A., Chaboyer, B., Jevremović, D., et al. 2008, *ApJS*, 178, 89
 Drawin, H.-W. 1968, *Zeitschrift für Physik*, 211, 404
 Drawin, H. W. 1969, *Zeitschrift für Physik*, 225, 483
 Frebel, A., Casey, A. R., Jacobson, H. R., et al. 2013, *ApJ*, 769, 57
 Fuhr, J. R., & Wiese, W. L. 2006, *Journal of Physical and Chemical Reference Data*, 35, 1669
 Kervella, P., Thévenin, F., Di Folco, E., et al. 2004, *A&A*, 426, 297
 Kervella, P., & Fouqué, P. 2008, *A&A*, 491, 855
 Kervella, P., Bigot, L., Gallenne, A., et al. 2017, *A&A*, 597, A137
 Koch, A., & McWilliam, A. 2014, *A&A*, 565, A23
 Kovalev, M., Bergemann, M., Ting, Y.-S., et al. 2019, *A&A*, 628, A54

Kurucz, R. L. 2005, *Memorie della Societa Astronomica Italiana Supplementi*, 8, 14
 Gaia Collaboration, Prusti, T., de Bruijne, J. H. J., et al. 2016, *A&A*, 595, A1
 Gaia Collaboration, Brown, A. G. A., Vallenari, A., et al. 2018, *A&A*, 616, A1
 García Pérez, A. E., Allende Prieto, C., Holtzman, J. A., et al. 2016, *AJ*, 151, 144
 González Hernández, J. I., & Bonifacio, P. 2009, *A&A*, 497, 497
 Gruyters, P., Lind, K., Richard, O., et al. 2016, *A&A*, 589, A61
 Gustafsson, B., Edvardsson, B., Eriksson, K., et al. 2008, *A&A*, 486, 951
 Johnson, J. A. 2002, *ApJS*, 139, 219
 Jönsson, H., Allende Prieto, C., Holtzman, J. A., et al. 2018, *AJ*, 156, 126
 Hannaford, P., Lowe, R. M., Grevesse, N., et al. 1992, *A&A*, 259, 301
 Harris, W. E. 1996, *AJ*, 112, 1487
 Hayek, W., Asplund, M., Carlsson, M., et al. 2010, *A&A*, 517, A49
 Heise, C., & Kock, M. 1990, *A&A*, 230, 244
 Kirby, E. N., Guhathakurta, P., Bolte, M., et al. 2009, *ApJ*, 705, 328
 Kroll, S., & Kock, M. 1987, *A&AS*, 67, 225
 Lambert, D. L., Heath, J. E., Lemke, M., et al. 1996, *ApJS*, 103, 183
 Landolt, A. U. 1992, *AJ*, 104, 340
 Lind, K., Bergemann, M., & Asplund, M. 2012, *MNRAS*, 427, 50
 Lovisi, L., Mucciarelli, A., Lanzoni, B., et al. 2013, *ApJ*, 772, 148
 Ludwig, H.-G., Caffau, E., Steffen, M., et al. 2009, *Mem. Soc. Astron. Italiana*, 80, 711
 Magic, Z., Collet, R., Asplund, M., et al. 2013, *A&A*, 557, A26
 Martin, G. A., Fuhr, J. R., & Wiese, W. L. 1988, *New York: American Institute of Physics (AIP) and American Chemical Society*, 1988
 Mashonkina, L. I., Sitnova, T. N., & Pakhomov, Y. V. 2016, *Astronomy Letters*, 42, 606
 Masseron, T., García-Hernández, D. A., Mészáros, S., et al. 2019, *A&A*, 622, A191
 McCall, M. L. 2004, *AJ*, 128, 2144
 Meléndez, J., & Barbuy, B. 2009, *A&A*, 497, 611
 Monaco, L., Bellazzini, M., Bonifacio, P., et al. 2005, *A&A*, 441, 141
 Mészáros, S., Martell, S. L., Shetrone, M., et al. 2015, *AJ*, 149, 153
 Mészáros, S., Masseron, T., García-Hernández, D. A., et al. 2020, *MNRAS*, 492, 1641
 Mucciarelli, A., Pancino, E., Lovisi, L., Ferraro, F. R., & Lapenna, E., 2013, *ApJ*, 766, 78
 Mucciarelli, A., Bellazzini, M., Catelan, M., et al. 2013, *MNRAS*, 435, 3667
 Mucciarelli, A., 2013, *arXiv1311.1403*
 Mucciarelli, A., Lapenna, E., Massari, D., Ferraro, F. R., & Lanzoni, B. 2015, *ApJ*, 801, 69
 Mucciarelli, A., Lapenna, E., Lardo, C., et al. 2019, *ApJ*, 870, 124
 Nidever, D. L., Hesselquist, S., Hayes, C. R., et al. 2019, *arXiv e-prints*, arXiv:1901.03448
 Plez, B. 2012, *Turbospectrum: Code for spectral synthesis*, ascl:1205.004
 Raassen, A. J. J., & Uylings, P. H. M. 1998, *A&A*, 340, 300
 Ruchti, G. R., Bergemann, M., Serenelli, A., et al. 2013, *MNRAS*, 429, 126
 Sbordone, L., Bonifacio, P., Castellì, F., & Kurucz, R. L. 2004, *Memorie della Societa Astronomica Italiana Supplementi*, 5, 93
 Ramírez, I., & Meléndez, J. 2005, *ApJ*, 626, 446
 Schlafly, E. F., & Finkbeiner, D. P. 2011, *ApJ*, 737, 103
 Skrutskie, M. F., Cutri, R. M., Stiening, R., et al. 2006, *AJ*, 131, 1163
 Stetson, P. B., & Pancino, E., *PASP*, 120, 1332
 Stetson, P. B., Pancino, E., Zocchi, A., Sanna, N., & Monelli, M. 2019, *MNRAS*, 485, 3042
 Yong, D., Norris, J. E., Bessell, M. S., et al. 2013, *ApJ*, 762, 26
 Wenger, M., Ochsenbein, F., Egret, D., et al. 2000, *A&AS*, 143, 9